Research Square

Preprints are preliminary reports that have not undergone peer review.
They should not be considered conclusive, used to inform clinical practice,
or referenced by the media as validated information.

Universal RKKY-like Interactions Between Tilted Skyrmions in Chiral Magnets

X. R. Wang

phxwan@cuhk.edu.cn

The Chinese University of Hong Kong, Shenzhen https://orcid.org/0000-0002-8600-3258

Xuchong Hu

The Chinese University of Hong Kong，Shenzhen https://orcid.org/0000-0002-4029-8310

Huaiyang Yuan

Article

Keywords:

Posted Date: June 22nd, 2026

DOI: https://doi.org/10.21203/rs.3.rs-9954563/v1

License: This work is licensed under a Creative Commons Attribution 4.0 International License.
Read Full License

Additional Declarations: There is **NO** Competing Interest.

Universal RKKY-like Interactions Between Tilted Skyrmions in Chiral Magnets

Skyrmion-skyrmion interaction is a fundamental problem that remains inadequately understood. Here we demonstrate that the interaction between two tilted skyrmions in a chiral magnetic film is intrinsically anisotropic, non-central, and oscillatory. This interaction varies periodically from repulsion to attraction with the skyrmion-skyrmion separation along a specified direction, resembling the Ruderman-Kittel-Kasuya-Yosida (RKKY) interaction observed between localized spins in metals. Our analysis reveals the underlying physics of a previously unrecognized universal wavy tail in the skyrmion spin texture. Importantly, the resulting RKKY-like interaction is universal for all tilted skyrmions, regardless of whether the tilt arises from an external field or crystalline magnetic anisotropy. These findings introduce a novel physical principle for designing skyrmion molecules or skyrmion superstructures, which have significant potential for applications in skyrmion-based spintronics and neuromorphic computing.

Magnetic skyrmions are localized spin structures that are topologically non-trivial [1]. Since their discovery [2–7], significant research has explored their fascinating physics and potential applications. This includes studies on skyrmion creation and annihilation [8–15], morphology [16–25], dynamics under various stimuli [26–34], skyrmion-skyrmion interactions, [35–49] as well as their possible usages in technology [50–52].

It is well known that two isolated skyrmions in vertically magnetized chiral films always repel each other [35–40]. However, recent studies have found that skyrmions can attract each other under a tilted external fields [41–43], or through thermal frustration [44], or by varying sample thickness [45, 46], and or through frustrated exchange interactions [47–49]. Despite of all progress, the underlying physics of these interactions remains poorly understood, and a clear understanding of the conditions under which two skyrmions in a chiral film can attract each other is still lacking.

In this article, we demonstrate that skyrmion–skyrmion interactions in tilted (from the film perpendicular direction) magnetized chiral films, caused by either a tilted magnetic field or a magnetic anisotropy, are non-central and intrinsically Ruderman-Kittel-Kasuya-Yosida-type (RKKY-type), periodically alternating between attraction and repulsion, due to the inherent periodic spin structure of the skyrmion tail if the tilted angle of magnetic easy-axis (from the perpendicular direction) is beyond a critical value. When two skyrmions are aligned along this periodic direction and separated by an integer multiple of the period, their wavy tails coincide, resulting in an energy reduction and an attractive interaction. Conversely, at separations of half-integer multiples of the period, the two tails are out of phase, and significant deformation is needed in order for two skyrmions to smoothly connect each other, leading to an increase in total energy and a repulsive force. These findings provide new insights into the nature of skyrmion–skyrmion interactions and open up avenues for skyrmion engineering in spintronics applications.

Model

A chiral magnetic film of thickness d lying in the xy-plane is modeled by a free energy E, which consists of an exchange energy of $E_{\rm ex} = \frac{Ad}{2}\int |\nabla \mathbf{m}|^2 \,\mathrm{d}^2\mathbf{x}$, where the exchange stiffness $A = 30\,\mathrm{pJ/m}$ is fixed and $\mathbf{m}$ is the direction of magnetization whose magnitude is $M_s = 1\,\mathrm{MA/m}$; a Dzyaloshinskii–Moriya interaction (DMI) energy of $E_{\rm DM} = \frac{Dd}{2}\int [\mathbf{m}\cdot(\nabla\times\mathbf{m})]\,\mathrm{d}^2\mathbf{x}$ with DMI strength $D = 4\,\mathrm{mJ/m^2}$; an anisotropy energy of $E_{\rm an} = d\int -\frac{K}{2}(m_y\sin\theta + m_z\cos\theta)^2\mathrm{d}^2\mathbf{x}$ where K is the anisotropy constant along the easy axis in the yz-plane, determined by the angle θ; a magnetic dipolar energy which adds to anisotropy by a term of $\frac{\mu_0 M_s^2 m_z^2}{2}$ with μ_0 being the vacuum permeability; and the Zeeman energy of $E_{\rm Ze} = -\mu_0 M_s d\int \mathbf{H}\cdot\mathbf{m},\mathrm{d}^2\mathbf{x}$, where $\mathbf{H}$ is the external magnetic field. In this study, only K, θ, and $\mathbf{H}$ vary to model different situations. Two cases are considered. The first one is $\mathbf{H}$-controlled anisotropy, where we set $\theta = 0$ and $K = 1.256\,\mathrm{MJ/m^3}$ to cancel the shape anisotropy, making the easy axis asymmetrical and preferably aligning spins along $\mathbf{H}$. The other is crystalline anisotropy with proper K and θ and $\mathbf{H} = 0$, resulting in a symmetrical axis. The results of the second case are primarily presented in the Supplementary Notes 1 [56].

Results

Interaction energy between two in-plane skyrmion. The nature of skyrmion interactions is given by the negative spatial gradient of two-skyrmion energy. We start with two 10 nm nucleation domains of $\mathbf{m} = (0, 1, 0)$ embedded in the ferromagnetic background state of $\mathbf{m} = (0, -1, 0)$ in a film of size $600\,\mathrm{nm}\times 600\,\mathrm{nm}\times 0.5\,\mathrm{nm}$. One domain is centered at the sample center $(0, 0)$ and the other at (x, y). The central spins at $(0, 0)$ and (x, y) are fixed and remaining spins in the film vary with time according to the Landau–Lifshitz–Gilbert (LLG) equation. The system settles into the stable configuration of two skyrmions centered at $(0, 0)$ and (x, y), respectively [19, 21]. We numerically confirm that the topological charge Q of each skyrmions defined as $Q = \frac{1}{4\pi}\iint \mathbf{m}\cdot(\partial_x\mathbf{m}\times\partial_y\mathbf{m})\mathrm{d}^2\mathbf{x}$ are 1. Figure 1(a) is the energy surface $E(x, y)$ of the two skyrmions when an external field of $H = 0.164\,\mathrm{T}$ is applied along the $-y$-direction. In the figure, E is set to zero when two skyrmions are infinitely far apart . It is sufficient to plot $E(x, y)$ in just one quadrant because of the symmetry of $E(\pm x, \pm y) = E(x, y)$. Notably, $E(x, y)$, or the skyrmion interaction, is anisotropic and non-central. Along the x-axis ($y = 0$), the energy decreases monotonically with x (black line in Fig. 1(b)), implying a repulsive force. In contrast, along the y-axis ($x = 0$), the energy profile exhibits RKKY-like oscillatory behaviour with multiple energy minima at $y_{min} = 66.5, 156.5, 247.5\,\mathrm{nm}$ (red line in Fig. 1(b)), indicating an alternating attractive and repulsive interactions between the two skyrmions. In other directions, oscillatory behaviour persists with the period of $\lambda/\sin\phi$, where ϕ is the angle between the skyrmion-skyrmion displacement (x, y) and y-axis, $\lambda \approx 156.5 - 66.5 \approx 247.5 - 156.5 \approx 90 \sim 91\,\mathrm{nm}$ which is not sensitive to H and ϕ. The blue curve in Fig. 1(b) is the energy variation along $y = x$ direction. According to energy surface $E(x, y)$, the skyrmion centered at (x, y) will relax to its local minimum at $(0, y_{min})$ when the skyrmion is allowed to move. The interaction is non-central if $x \neq 0$ and skyrmion trajectory on its way to the nearby energy minimum is curved. Which y_{min} being end up with depends on the initial location of the skyrmion (see the Supplementary Note 2[56]).

Periodic tail structure. To reveal the origin of the

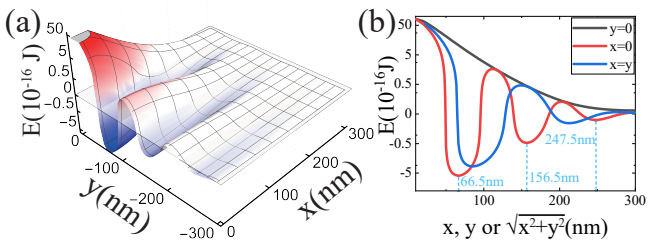


Figure 1. (a) Energy surface $E(x, y)$ of two skyrmions for $H = 0.164$T along the y-axis. $E = 0$ is chosen for two isolated skyrmions infinitely apart. (b) $E(x, y)$ as a function of x along $y = 0$ (black line), or y along $x = 0$ (red line), or $\sqrt{x^2 + y^2}$ along $y = x$ (blue line). The vertical blue dash-lines indicate local minima.

oscillatory attraction-repulsion interaction, we compare the spin structures of an isolated perpendicular skyrmion with that of an in-plane skyrmion. Figure 2(a) shows an isotropic spin structure of a perpendicular skyrmion of topological charge 1. In the polar coordinate of (ρ, ϕ), the polar angle Θ of $\mathbf{m}$ (angle between $\mathbf{m}$ and z-axis) depends only on ρ while the azimuthal angle Φ (the angle between the x-axis and the projection of $\mathbf{m}$ in the xy-plane) depends only on ϕ as shown in Fig. 2(b): $\Theta(\rho)$ (red) for $\phi = 0$ (stars), 40^0 (squares), 70^0 (triangles) and $\Phi(\phi)$ (blue) for $\rho = 10$nm (stars), 40nm (squares), 70nm (triangles). The perfect overlap of $\Theta(\rho)$ and $\Phi(\phi)$ confirm the isotropic spin structure. In contrast, the spin structure of an in-plane skyrmion of topological charge 1 centered at $(0, 0)$ (when the external field is along the $-y$-direction) is anisotropic as plotted in Fig.2(c) (red and blue for $m_z \geq 0.5$ and $m_z \leq -0.5$, respectively). The skyrmion has a stripy spin structure, overall along the x-axis, with a well-defined period as shown in the inset of Fig.2(c): red for $m_x > 0$ and blue for $m_x < 0$. The stripy structure can also be seen from $m_x(y)$ (the red curves) and $m_z(y)$ (the blue curves) for a fixed x, exhibiting oscillatory behaviour as shown in Fig.2(d).

To see whether the periodical stripy tail of an in-plane skyrmion is intrinsic or not, we go back to the equations of stable spin textures [25]. For the easy-axis controlled by $\mathbf{H}$ in the yz-plane, Θ is defined as the angle between $\mathbf{m}$ and the easy-axis (defined as z'-axis with y'-axis in the yz-plane), and Φ the angle between the x'-axis (perpendicular to yz-plane) and the projection of $\mathbf{m}$ to the plane perpendicular to the easy-axis. In terms of $\kappa' \equiv \pi^2 D^2/(8\mu_0 M_s A H)$ and using nature length unit of $4A/\pi D$, equations for Θ and Φ are [21–23],

$$2\nabla^2\Theta - \sin 2\Theta\,(\nabla\Phi)^2 + \frac{4}{\pi}[\sin\theta_H \sin 2\Theta\partial_y\Phi + 2\sin^2\Theta(\cos\Phi\partial_x\Phi + \cos\theta_H \sin\Phi\partial_y\Phi)] + \frac{2}{\kappa'}\sin\Theta = 0 \tag{1}$$

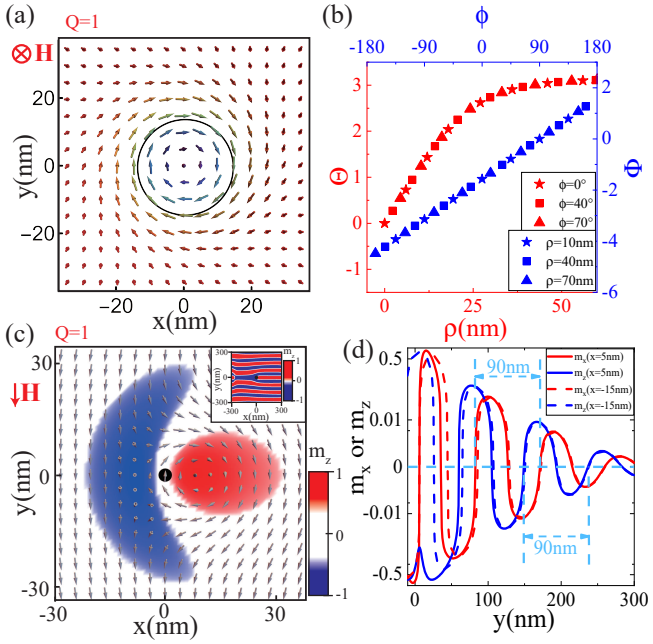


Figure 2. (a) A perpendicular skyrmion with $H = 0.164$T along the $-z$-axis. (b) $\Theta(\rho)$ (red) for $\phi = 0$ (stars), 40^0 (squares), 70^0 (triangles) and $\Phi(\phi)$ (blue) for $\rho = 10$nm (stars), 40nm (squares), 70nm (triangles). (c) An in-plane skyrmion $H = 0.164$T along the $-y$-axis. Inset: regions of $m_z > 0$ (red) and $m_z < 0$ (blue). The skyrmion center is indicated by a dot. (d) m_x (red) and m_z (blue) as a function of y for $x = 5$nm (solid curve) and -15 nm (dashed lines).

$$-\sin 2\Theta\,(\nabla\Theta)\cdot(\nabla\Phi) - \sin^2\Theta\nabla^2\Phi + \frac{2}{\pi}[\sin\theta_H \sin 2\Theta\partial_y\Theta + 2\sin^2\Theta(\cos\Phi\partial_x\Theta + \cos\theta_H \sin\Phi\partial_y\Theta)] = 0, \tag{2}$$

where θ_H is the angle between $\mathbf{H}$ and the z-axis. The derivation is presented in the Supplementary Material[56]. For $\theta_H = \pi/2$ and $\Theta(0, 0) = 0$, $\Theta(|x| \to \infty, or|y| \to \infty) = \pi$. Far from the skyrmion center, $\Theta' \equiv \pi - \Theta(x, y) \ll 1$, (1) and (2), linear in Θ', are,

$$\nabla^2\Theta' - \Theta'\left[(\nabla\Phi)^2 - \frac{4}{\pi}\partial_y\Phi + \frac{1}{\kappa'}\right] = 0, \tag{3}$$

$$\nabla\Theta'\cdot\nabla\Phi - \frac{2}{\pi}\partial_y\Theta' + \frac{\Theta'}{2}\nabla^2\Phi = 0. \tag{4}$$

For $\kappa' < \pi^2/4$, the solutions of (3) and (4) are,

$$\Theta(x, y) = \pi - \pi e^{-k_x|x| - k_y|y|},\ \Phi(y) = \frac{2}{\pi}y + \Phi_0, \tag{5}$$

with real k_x and k_y where $k_x^2 + k_y^2 = 1/\kappa' - 4/\pi^2$, and Φ_0 is a constant. The skyrmion is metastable for $\kappa' < \pi^2/4$, otherwise unstable. Thus, the tails of any localized spin textures in tilted chiral magnetic films must be corrugated, as reported for conical state [7] and domain wall [57], see the Supplementary Note 4[56]

for details. Although k_x^{-1} and k_y^{-1} depend on model parameter κ' (or $\kappa \equiv \pi^2 D^2/(16AK)$ in the absence of a magnetic field and in an in-plane magnetized film, see Supplementary Note 3[56] for details, period λ of Φ (the wavy or corrugated tail) depends only on the length scale of $4A/\pi D$ as $\lambda = 2\pi\left(\frac{2}{\pi}\right)^{-1} \times \frac{4A}{\pi D} = 4\pi\frac{A}{D} \approx 93\,\text{nm}$, not sensitive to the field strength (or magnetic anisotropy)! The approximate value agrees well with the simulated value of $90 \sim 91\,\text{nm}$ from Mumax3. For a perpendicular skyrmion under a perpendicular field, similar analysis does not have a wavy tail structure.

Attractive interaction from the wavy tail. The wavy tails give rise to an anisotropic, non-central, and oscillatory interaction between two tilted skyrmions. The interaction has a well-defined period λ in skyrmion-skrymion separation. Consider one skyrmion centered at $(0,0)$ and the other at $(0,y)$, two skyrmion tails in the overlapped region are the same when $y = n\lambda$, and two skyrmions can share the same tail and save one tail formation energy. This energy reduction can bind two skyrmions together, similar to the formation of a molecule from atoms. This energy deduction can be estimate from skyrmion profile of Eq. (5) as,

$$\begin{aligned}\frac{\Delta E}{Ad} &= \int_{n\lambda/2}^{\infty} \mathrm{d}\mathbf{y} \int_{-\infty}^{\infty} \mathrm{d}\mathbf{x}\Big[(\nabla\Theta)^2 + \Theta^2 (\nabla\Phi)^2 - \\ &\quad - \frac{4\Theta^2}{\pi}\partial_y\Phi + \frac{\Theta^2}{\kappa'} + \Theta^2\cos\Phi\partial_x\Theta\Big] \qquad (6)\\ &= \left(\frac{4(k_x^2+k_y^2)}{k_x k_y} - \frac{4k_y}{\pi k_y^2 + \frac{4}{\pi}}\right) e^{-k_y n\lambda} > 0.\end{aligned}$$

In the case of $y = (n+1/2)\lambda$, the two wavy tails are out of phase. To smoothly connecting two skyrmions together, both skyrmions must deform their structures that require an increase of the total energy, resulting in a repulsive force.

To further support our assertion of attraction from the match of two skyrmion tails, we compare Φ in the overlapped region of two independent skyrmions at a fixed separation, one at $(0,0)$ and the other at (x_0,y_0), as well as the Φ of fully related structure of the biskyrmion. We first use Mumax3 to simulate only one skyrmion centered at $(0,0)$ with the model parameters specified above and compute $\Phi(l)$ [red symbols in Figs. 3(a)-(b)], where $l \equiv |\sqrt{x_0^2+y_0^2}(|y|/|y_0| - 1/2)$ measures distance from the middle point between the two skyrmions along the line of $y = (y_0/x_0)x$. Then, we simulate only one skyrmion centered at (x_0,y_0) for its $\Phi(l)$ [blue symbols in Figs. 3(a)-(b)]. Finally, we simulate a bi-skyrmion molecule, or two bonded skyrmions respectively centered at $(0,0)$ and (x_0,y_0) and compute $\Phi(l)$ [black dashed lines in Figs. 3(a)-(b)]. Spin structure of two skyrmions separated by the distance corresponding to the first energy minimum is presented in Supplementary Note 6 [56]. Figure 3(a) presents $\Phi(l)$ when two tails are in good match or two skyrmions attract each other for $(x_0,y_0) = (0,66\text{nm})$, $(100\text{nm},66\text{nm})$, and $(-200\text{nm},67\text{nm})$. $\Phi(l)$ is linear in l with the expected slop of $\frac{D}{2A} = 0.0667\,\text{nm}^{-1}$. The difference in $\Phi(l)$ among two independent skyrmions and the bi-skyrmion molecule can hardly been seen, showing small deformation of the bi-skyrmion molecule. The period of oscillatory stripy tail along direction of (x_0,y_0) is $\lambda/\cos(\phi)$ where $\phi = tan^{-1}(y_0/x_0)$. $(x_0,y_0) = (0,66\text{nm})$ is slightly different from the first minimum of $(0,66.5\text{nm})$ due to a small deformation of two skyrmions from the isolated ones.

In the opposite case when two skyrmions repel each other, their tails in the overlapped region are out of phase, or the difference between two Φ's is π as shown in Fig. 3(b) for $(x_0,y_0) = (0,113\text{nm})$, $(100\text{nm},113\text{nm})$, and $(-200\text{nm},113\text{nm})$ which are close to the peaks of total energy in Fig. 1(a). For all three cases, $\Phi(l)$ of the skyrmion centered at $(0,0)$ differs from $\Phi(l)$ of the skyrmion centered at (x_0,y_0) by π for all l. Furthermore, the same as the first case, $\Phi(l)$ is linear of slop $\frac{D}{2A}$. Because of the mismatch of the two tails, spin structures of bi-skyrmion in the overlapped region must greatly deform from the single skyrmion structure and $\Phi(l)$ of relaxed bi-skyrmion should be different from the values of single skyrmion. Indeed, as shown in Fig. 3(b), $\Phi(l)$ of fully relaxed spin structure of two skyrmions centered at $(0,0)$ and (x_0,y_0), respectively, are not only different from both red and blue symbols, but also not linear any more.

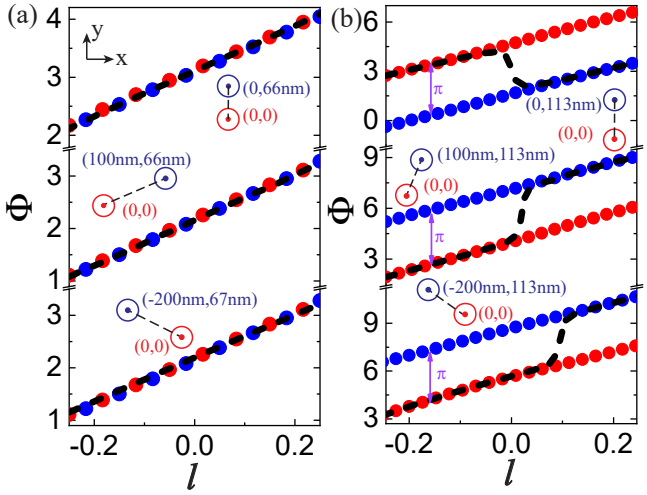


Figure 3. $\Phi(l)$ of skyrmion centered at $(0,0)$ (red symbols) and (x_0,y_0) (blue symbols), and $\Phi(l)$ of the two coupled skyrmions (black dashed line) for $(x_0,y_0) = (0,66\text{nm})$, $(100\text{nm},66\text{nm})$, and $(-200\text{nm},67\text{nm})$ (a) and for $(x_0,y_0) = (0,113\text{nm})$, $(100\text{nm},113\text{nm})$, and $(-200\text{nm},113\text{nm})$ (b).

Phase diagram. We have seen that the interactions between two perpendicular skyrmions and between two in-plane skyrmions are fundamentally different. A natural question is what in between. Namely, is skyrmion-skyrmion interaction RKKY-like if the easy axis is in an arbitrary direction in the yz-plane? This question can be easily investigated by changing θ_H. According to Eqs. (1) and (2), stable spin textures are fully determined by

θ_H and κ'. Our Mumax3 simulations lead to the phase diagram of Figs. 4(a) in the $\kappa' - \theta_H$ plane that distinguish three phases: RKKY-like skyrmion-skyrmion interaction (the red); repulsive skyrmion-skyrmion interaction (the green); and region without isolated skyrmion (the orange and $\kappa' > 4$). Interestingly, RKKY-like interaction appears only when $\theta_H > 23°$. From the analysis of Eqs. (1) and (2), boundary between the red and orange is given by $\kappa' = \{\pi/[2\sin(\theta_H)]\}^2$ (grey curve) which agree excellently with the simulations (Supplementary Note 4 [56]).

Although results presented so far are all from asymmetrical anisotropy due to **H**. A natural question is whether they are also true to the case of usual symmetric crystalline magnetic anisotropy. We have carried out similar studies in the absence of $\mathbf{H} = 0$ and in the presence a proper K to address the issue by varying θ. Similar equations like Eqs. (1) and (2) can be obtained which depend only on θ and $\kappa \equiv (\pi^2 D^2)/(16AK)$, i.e. stable spin textures are uniquely determined by these two parameters. Figure 4(b) is the phase diagram in the $\kappa - \theta$ plane. Interestingly and surprisingly, RKKY-like interaction again appears only for $\theta > 23°$ and $\kappa < 1$ for isolated skyrmion, in agreement with previous results [18, 19, 24]. The details results are presented in Supplementary Note 1 [56]. Furthermore, the physics presented here does not change if one uses interfacial DMI (see Supplementary Note 5 [56]), rather than the bulk DMI present above. As expected, results presented here do not depend on the origins of the anisotropy, nature of the anisotropy-symmetric or asymmetric, or the type of DMIs.

With tunable skyrmion-skyrmion interactions, one can design more complicated skyrmion superstructures. Below, we demonstrate that a bi-skyrmion molecule binding together by the attraction moves as one object under a spin-orbit torque acting only on one part of the molecule. Figure 4(c) plots the trajectories of the molecule consisting two skyrmions located on opposite sides of $y = 0$ and separated by a distance of 66.5 nm. A spin–orbit torque from a current density of 10^{11} A/m^2 acting only on the skyrmion in $y > 0$ region. Notably, two skyrmions move together and maintain their bond length of 66.5 nm during the whole process.

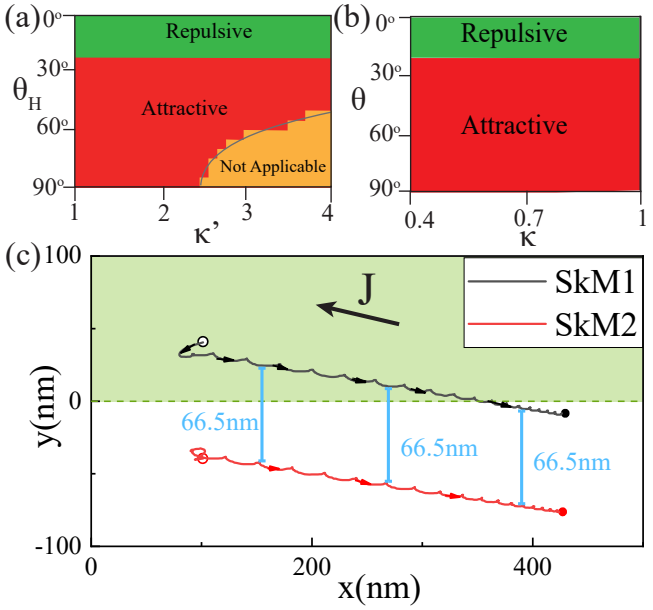


Figure 4. Phase diagrams of RKKY-like interaction (the red), repulsive interaction (the green) , and non-existence of isolated skyrmion (the orange) in $\kappa' - \theta_H$ plane for **H** controlled asymmetric anisotropy (a) and in $\kappa - \theta$ planes for $K - \theta$ controlled symmetric magnetic anisotropy (b). (c) Trajectories of a bi-skyrmion molecule under a spin–orbit torque. Torque is applied only on the top skyrmion whose motion drags the other skyrmion to move together.

Conclusions

In conclusion, skyrmions in a tilted magnetic field or in a tilted magnetic anisotropy with a sufficient large component in the film plane are anisotropic and have periodically wavy tails. This wavy tail leads to skyrmion attraction when the two tails match with each other in the overlapped region, and repulsion when their tails mismatch with each other. As a result, two tilted skyrmions exhibit RKKY-like interaction, oscillating between attraction and repulsion with a period that is determined by the period of wavy tail. The period is proportional to A/D and inversely proportional to $\sin\theta_H$ (for field-controlled anisotropy) or $\sin\theta$ (for crystalline anisotropy). The direction of periodical tail structure is determined by the types of DMIs and easy axis direction (see Supplementary Note 5 [56]).

Anisotropic and oscillatory skyrmion interaction gives rise to new possibilities in skyrmion-based spintronics. The presence of multiple optimal skyrmion–skyrmion separations offers an additional degree of freedom for controlling the dynamics of isolated skyrmions. Our findings thus open a promising avenue for advanced skyrmion manipulation such as creating skyrmion molecules or more complicated superstructures.

Methods

Numerical simulation. Magnetization dynamics is governed by the LLG equation:

$$\frac{\partial \mathbf{m}}{\partial t} = -\gamma\, \mathbf{m} \times \mathbf{H}_{\text{eff}} + \alpha\, \mathbf{m} \times \frac{\partial \mathbf{m}}{\partial t}, \qquad (7)$$

where γ is the gyromagnetic ratio and α is the Gilbert damping. The effective field is $\mathbf{H}_{\text{eff}} = -\delta E/\delta \mathbf{m} = A/(\mu_0 M_s)\nabla^2 \mathbf{m} + K(m_z \cos\theta + m_y \sin\theta)(\cos\theta \mathbf{z} + \sin\theta \mathbf{y}) - D/(\mu_0 M_s)\nabla \times \mathbf{m} + \mathbf{H}$. To obtain the total energy and stable spin structures of two skyrmions centered at two fixed locations, we use Mumax3 package [53] to numerically solve the LLG equation by fixing the spins at skyrmion centers and with meshsize of 1 nm × 1 nm × 0.5 nm. The film size and meshsize used in our numerical simulations are sufficient to obtain accurate results (see Supplementary Note 2 [56]).

[1] Bogdanov, A. N. & Rößler, U. K. Chiral symmetry breaking in magnetic thin films and multilayers. *Phys. Rev. Lett.* **87**, 037203 (2001).

[2] Mühlbauer, S. *et al.* Skyrmion Lattice in a Chiral Magnet *Science* **323**, 915 (2009).

[3] Yu, X. Z. *et al.* Near room-temperature formation of a skyrmion crystal in thin-films of the helimagnet FeGe. *Nat. Mater.* **10**, 106 (2011).

[4] Woo, S. *et al.* Observation of room-temperature magnetic skyrmions and their current-driven dynamics in ultrathin metallic ferromagnets. *Nat. Mater.* **15**, 501 (2016).

[5] Boulle, O. *et al.* Room-temperature chiral magnetic skyrmions in ultrathin magnetic nanostructures. *Nat. Nanotech.* **11**, 449 (2016).

[6] Kézsmárki, I. *et al.* Néel-type skyrmion lattice with confined orientation in the polar magnetic semiconductor GaV_4S_8. *Nat. Mater.* **14**, 1116 (2015).

[7] Munzer, W. *et al.* Observation of magnetic excitations of skyrmion crystal in a helimagnetic insulator Cu_2OSeO_3. *Phys. Rev. B* **81**, 041203 (2010).

[8] Back, C. *et al.* The 2020 skyrmionics roadmap. *J. Phys. D* **53**, 363001 (2020).

[9] Rößler, U. K., Bogdanov, A. N., and Pfleiderer, C. Spontaneous skyrmion ground states in magnetic metals *Nature* **442**, 797 (2006).

[10] Tchoe, Y. & Han, J. H. Skyrmion generation by current. *Phys. Rev. B* **85**, 174416 (2012).

[11] Nayak, A. K. *et al.* Magnetic antiskyrmions above room temperature in tetragonal Heusler materials. *Nature* **548**, 561 (2017).

[12] Jiang, W. *et al.* Blowing magnetic skyrmion bubbles. *Science* **93**, 283 (2015).

[13] Iwasaki, J., Mochizuki, M. & Nagaosa, N. Universal current-velocity relation of skyrmion motion in chiral magnets. *Nat. Commun.* **4**, 1 (2013).

[14] Hrabec, A. *et al.* Current-induced skyrmion generation and dynamics in symmetric bilayers. *Nat. Commun.* **8**, 1 (2017).

[15] Jin, C., Song, C., Wang, J. & Liu, Q. Dynamics of antiferromagnetic skyrmion driven by the spin Hall effect. *Appl. Phys. Lett.* **09**, 182404 (2016).

[16] Wu, Y. Z. *et al.* Magnetic stripe domains in coupled magnetic sandwiches. *Phys. Rev. Lett.* **93**, 117205 (2004).

[17] Dho, J., Kim, Y. N., Hwang, Y. S., Kim, J. C. & Hur, N. H. X-ray studies of aligned magnetic stripe domains in perpendicular multilayers. *Phys. Rev. B* Condens. Matter **336**, 136 (2003).

[18] Wang, X. R., Hu, X. C., & Wu, H. T. Stripe skyrmions and skyrmion crystals. *Commun. Phys.* **4**, 142 (2021).

[19] Wu, H. T., Hu, X. C., Jing, K. Y. & Wang, X. R. Size and profile of skyrmions in skyrmion crystals. *Commun. Phys.* **4**, 210 (2021).

[20] Wu, H. T., Hu, X. C. & Wang, X. R. Nematic and smectic stripe phases and stripe-SkX transformations. *Sci. China-Phys. Mech. Astron.* **65**, 247512 (2022).

[21] Hu, X. C., Wu, H. T. & Wang, X. R. A theory of skyrmion crystal formation. *Nanoscale* **14**, 7516 (2022).

[22] Wang, X. R. & Hu, X. C. Particle-continuum duality of skyrmions. *Phys. Rev. B* **107**, 174412 (2023).

[23] Wang, X. R., Hu, X. C. & Sun, Z. Z. Topological Equivalence of Stripy States and Skyrmion Crystals *Nano Lett.* **23**, 3954 (2023).

[24] Wijethunga, M. V., Hu, X. C., & Wang, X. R. Phase-diagram of condensed and isolated skyrmions in chiral magnetic films. *Commun. Phys.* **8**, 123 (2025).

[25] Wang, X. S., Yuan, H. Y. & Wang, X. R. A theory on skyrmion size. *Commun. Phys.* **1**, 1 (2018).

[26] Schütte, C., Iwasaki, J., Rosch, A. & Nagaosa, N. Inertia, diffusion, and dynamics of a driven skyrmion. *Phys. Rev. B* **90**, 174434 (2014).

[27] Yuan, H. Y., Wang, X. S., Yung, M. H. & Wang, X. R. Wiggling skyrmion propagation under parametric pumping. *Phys. Rev. B* **99**, 014428 (2019).

[28] Gong, X., Yuan, H. Y., & Wang, X. R. Current-driven skyrmion motion in granular films. *Phys. Rev. B* **101**, 064421 (2020).

[29] Yu, X. Z. *et al.* Skyrmion flow near room temperature in an ultralow current density. *Nat. Commun.* **3**, 1 (2012).

[30] Neubauer, A. *et al.* Topological Hall effect in the A phase of MnSi. *Phys. Rev. Lett.* **102**, 186602 (2009).

[31] Lee, M., Kang, W., Onose, Y., Tokura, Y. & Ong, N. P. Unusual Hall effect anomaly in MnSi under pressure. *Phys. Rev. Lett.* **102**, 186601 (2009).

[32] Gong, X., Jing, K. Y., Lu, J. & Wang, X. R. Skyrmion pinning by disk-shaped defects. *Phys. Rev. B* **105**, 094437 (2022).

[33] Lin, S. Z., Reichhardt, C., Batista, C. D., & Saxena, A. Particle model for skyrmions in metallic chiral magnets: Dynamics, pinning, and creep. *Phys. Rev. B* **87**, 214419 (2013).

[34] Zang, J., Mostovoy, M., Han, J. H., & Nagaosa, N. Dynamics of Skyrmion Crystals in Metallic Thin Films. *Phys. Rev. Lett.* **107**, 136804 (2011).

[35] Zhang, X. *et al.* Skyrmion-skyrmion and skyrmion-edge repulsions in skyrmion-based racetrack memory. *Sci. Rep.* **5**, 1 (2015).

[36] Lin, S. Z., Reichhardt, C., Batista, C. D. & Saxena, A. Particle model for skyrmions in metallic chiral magnets: Dynamics, pinning, and creep. *Phys. Rev. B* **87**, 214419 (2013).

[37] Brearton, R., van der Laan, G. & Hesjedal, T. Magnetic skyrmion interactions in the micromagnetic framework. *Phys. Rev. B* **101**, 134422(2020).

[38] Capic, D., Garanin, D. A., & Chudnovsky, E. M. Skyrmion–skyrmion interaction in a magnetic film. *J. Condens. Matter Phys.* **32**, 415803(2020).

[39] Wang, Y., Wang, J., Kitamura, T., Hirakata1, H. & Shimada, T. Exponential temperature effects on skyrmion-skyrmion interaction. *Phys. Rev. Appl.* **18**, 044024 (2022).

[40] Lin, S. Z. & Hayami, S. Ginzburg-Landau theory for skyrmions in inversion-symmetric magnets with competing interactions. *Phys. Rev. B* **93**, 064430(2016).

[41] Lin, S. Z. & Saxena, A. Noncircular skyrmion and its anisotropic response in thin films of chiral magnets under a tilted magnetic field. *Phys. Rev. B* **92**, 180401 (2015).

[42] Kameda, M., Koyama, R., Nakajima, T., & Kawaguchi, Y. Controllable interskyrmion attractive interactions and resulting skyrmion-lattice structures in two-dimensional chiral magnets with in-plane anisotropy. *Phys. Rev. B* **104**, 174446 (2021).

[43] Tiwari, K. L., Lavoie, J., Pereg-Barnea, T. & Coish, W. A. Tunable skyrmion-skyrmion binding on the surface of a topological insulator. *Phys. Rev. B* **100**, 125414(2019).

[44] Leonov, A. O. & Rößler, U. K. Mechanism of skyrmion attraction in chiral magnets near the ordering tempera-

tures. *Nanomaterials* **13**, 891 (2023).
[45] Loudon,J. C., Leonov, A. O., Bogdanov, A. N., Hatnean, M. C. & Balakrishnan, G. Direct observation of attractive skyrmions and skyrmion clusters in the cubic helimagnet Cu2OSeO. *Phys. Rev. B* **97**, 134403 (2018).
[46] Du, H. *et al.* Interaction of individual skyrmions in a nanostructured cubic chiral magnet. *Phys. Rev. Lett.* **120**, 197203 (2018).
[47] Rózsa, L., Deák, A., Simon, E., Yanes, R., & Udvardi, L. Skyrmions with attractive interactions in an ultrathin magnetic film. *Phys. Rev. Lett.* **117**, 157205 (2016).
[48] Rózsa, L. *et al.* Skyrmions with Attractive Interactions in an Ultrathin Magnetic Film. *Phys. Rev. Lett.* **117**, 157205 (2016).
[49] Leonov, A. O. & Mostovoy, M. Multiply periodic states and isolated skyrmions in an anisotropic frustrated magnet. *Nat. Commun.* **6**, 8275 (2015).
[50] Tomasello, R. *et al.*A strategy for the design of skyrmion racetrack memories. *Sci. Rep.* **4**, 1 (2014).
[51] Kang, W. *et al.* Voltage controlled magnetic skyrmion motion for racetrack memory. *Sci. Rep.* **6**, 1 (2016).
[52] Luo, S. *et al.* Reconfigurable skyrmion logic gates. *Nano Lett.* **18**, 1180 (2018).
[53] Vansteenkiste, A. *et al.* The design and verification of MuMax3. *AIP. Adv.* **4**, 107133 (2014).
[54] Göbel, B., Henk, J., & Mertig, I. Forming individual magnetic biskyrmions by merging two skyrmions in a centrosymmetric nanodisk. *Sci. Rep.* **9**, 9521 (2019).
[55] Yu, X. Z. *et al.* Biskyrmion states and their current-driven motion in a layered manganite *Nat. Commun.* **5**, 3198 (2014).
[56] Supplementary Notes on the verification of numerical simulations, equations and solution for wavy tail with tilted field, tilted anisotropy, results for the interfacial DMI, and etc.
[57] Schoenherr P. *et al.* Topological domain walls in helimagnets *Nature Physics* **14**, 465 (2018).

Supplementary Files

This is a list of supplementary files associated with this preprint. Click to download.

- SupplementaryInformation.pdf